The Effect of Mesoporous Bioglass on Osteogenesis and Adipogenesis of Osteoporotic BMSCs

Tao Wu[1#], Ning Cheng[1,4#], Chun Xu[3#], Wei Sun[1,2], Chengzhong Yu[3] and Bin Shi[1,2*]

[1]The State Key Laboratory Breeding Base of Basic Science of Stomatology (Hubei-MOST) & Key Laboratory of Oral Biomedicine Ministry of Education, School & Hospital of Stomatology, Wuhan University, 237 Luoyu Road, Wuhan 430079, P. R. China

[2]Department of Dental Implantology, School and Hospital of Stomatology, Wuhan University, Wuhan, People's Republic of China, China

[3]Australian Institute for Bioengineering and Nanotechnology (AIBN), the University of Queensland, Brisbane, QLD 4067, Australia

[4]Oral Biology Curriculum, School of Dentistry, University of North Carolina at Chape l Hill, Chapel Hill, NC 27599, USA

E-mail: shibin_dentist@126.com (B. Shi)

Abstract

This study evaluated the effect of mesoporous bioglass (MBG) dissolution on the differentiation of bone marrow mesenchymal stem cells (BMSCs) derived from either sham control or ovariectomized (OVX) rats. MBG was fabricated by evaporation-induced self-assembly method. Cell proliferation was tested by Cell Counting Kit-8 assay, and cytoskeletal morphology was observed by fluorescence microscopy. Osteogenic differentiation was evaluated by alkaline phosphatase (ALP) staining and activity, Alizarin Red staining, while adipogenic differentiation was assessed by Oil Red-O staining. Quantitative real-time PCR and Western blot analysis were taken to evaluate the expression of runt-related transcription factor 2 (*Runx2*) and proliferator-activated receptor-γ (*PPARγ*). We found that MBG dissolution (0, 25, 50, 100, 200μg/ml) was nontoxic to BMSCs growth. Sham and OVX BMSCs exhibited the highest ALP activity in 50μg/ml of MBG osteogenic dissolution, except that sham BMSCs in 100μg/ml showed the highest ALP activity on day 14. *Runx2* was significantly upregulated after 100μg/ml of MBG stimulation in sham and OVX BMSCs for 7 and 14 days, except that 25μg/ml showed highest upregulation effect on

This article has been accepted for publication and undergone full peer review but has not been through the copyediting, typesetting, pagination and proofreading process which may lead to differences between this version and the Version of Record. Please cite this article as an 'Accepted Article', doi: 10.1002/jbm.a.35841

OVX BMSCs at day 7. *PPARγ* was downregulated after MBG stimulation. The protein level of Runx2 from the sham BMSCs group was significantly upregulated after lower doses (25 and 50μg/ml) of MBG stimulation, whereas PPARγ was downregulated in the sham and OVX BMSCs group. Thus, both the osteogenic and adipogenic abilities of BMSCs were damaged under OVX condition. Moreover, lower concentration of MBG dissolution can promote osteogenesis but inhibit adipogenesis of the sham and OVX BMSCs.

Key words

Mesoporous bioglass (MBG); Bone marrow mesenchymal stem cells (BMSCs); osteogenesis; adipogenesis; osteoporosis

Introduction

Bioactive glass (BG) was discovered in 1969 and is now widely applied in bone tissue regeneration because of their biocompatibility, osteoconduction, and osteoinduction properties [1,2]. Mesoporous bioglass (MBG) with an ordered mesopore channel structure elicits better performance as bone substitutes than BG, and this performance is attributed to a faster release of Ca, P, and Si ions and the porous structure of MBG [3,4]. MBG soaked in physiological fluid releases Ca^{2+} and Na^{+} exchange with H^{+} from the fluid to form a hydrated silica gel on the surface. This gel turns into an amorphous $CaO\text{-}P_2O_5\text{-}SiO_2$ layer with a continuously consumption of Ca^{2+} and PO_4^{3-}, and subsequently crystallizes into a hydroxycarbonate apatite (HCA) layer through constant incorporating with Ca^{2+}, PO_4^{3-}, OH^- and CO_3^{2-} [5,6] The growing HCA layer provides an ideal environment for osteoblasts colonization, proliferation and differentiation [7]. Our previously studies showed the importance of MBG during osteoblast differentiation and mineralization both *in vivo* and *in vitro* [8,9]. Other groups have also reported that the released soluble ions from bioglass can stimulate osteogenesis [10,11]. For instance, the dissolution media of 45S5 Bioglass® with Si ion concentration of 15 and 20μg/ml tends to promote osteoblast proliferation and differentiation[11]. However, the involved cellular mechanism was ambiguous, especially in bone disease such as osteoporosis.

Osteoporosis is a common bone disease among post-menopausal women and the aging population, characterized by poor bone strength, low bone mass and bone microarchitectural impairment [12]. Osteoporosis is induced by the disruption of bone remodeling resulting from an imbalance between bone formation and resorption [13]. The ovariectomized (OVX) animal model is widely used as a golden standard to study the pathophysiological conditions of postmenopausal osteoporosis [8,14,15]. Osteoporotic bone loss has been associated with increased adipogenesis in bone marrow post ovariectomy or glucocorticoid treatment [16,17].

Primary bone marrow mesenchymal stem cells (BMSCs) are widely used to study skeletal biology due to their potential to differentiate into mesodermal lineages such as osteoblasts, chondrocytes and adipocytes [18-21]. BMSCs, which are vital components during new bone formation, can be easily accessed and they show a low risk of tumorigenesis after implantation [22]. Interestingly, osteoblasts and adipocytes share a common precursor in the bone marrow stroma, and the imbalance between BMSCs osteogenesis and adipogenesis can lead to osteoporosis [23]. Two main transcription factors namely, runt-related transcription factor 2 (Runx2) and peroxisome proliferator-activated receptor-γ (PPARγ), are generally regarded as the master regulators during osteogenesis and adipogenesis [24-26].

We fabricated MBG through an evaporation-induced self-assembly method [27]. MBG dissolution was diluted into different concentrations to investigate its effects on morphology, proliferation and differentiation of sham and OVX BMSCs. We also studied the expression patterns of Runx2 and PPARγ during osteogenesis and adipogenesis.

Materials and methods

2.1 Materials

Nonionic block copolymer EO20PO70EO20 (P123), tetraethyl orthosilicate (TEOS), Calcium nitrate tetrahydrate ($Ca(NO_3)_2 \cdot 4H_2O$), triethyl phosphate (TEP), FITC-phalloidin, β-glycerol phosphate, L-ascorbic acid, insulin, indometacin, dexamethasone and 1-methyl-3-isobutylxanthine were purchased from Sigma-Aldrich. Alizarin Red power, Oil Red-O power, *p*-nitrophenyl phosphate and *p*-nitrophenol were purchased from Aladdin. Penicillin/streptomycin (P/S) solution and α-MEM were purchased from HyClone. Fetal bovine serum (FBS) was purchased from Gibco. Triton X-100 was purchased from Amresco. DAPI was purchased from Beyotime. CCK-8 was purchased from Dojindo Molecular Technologies. ALP staining kit was purchased from Nanjing Jiangcheng Bioengineering Institute. PPARγ and Runx2

antibody were purchased from Cell Signaling Technology.

2.2 Preparation of mesoporous bioglass

MBG was synthesized using a reported evaporation-induced self-assembly process [28]. In a typical synthesis, 4.0 g P123, 6.7 g TEOS, 1.4 g $Ca(NO_3)_2 \cdot 4H_2O$, 0.73 g TEP and 1.0 g HCl (0.5 mM) were added into 60 g absolute ethanol and stirred in a 100 ml glass bottle for 1 day at 24 ℃. Then the mixture was transferred into a Petri Dish for the evaporation-induced self-assembling. The dried products were calcined at 700 ℃ for 5 h to obtain the final MBG. The feeding molar ratio of Si and Ca is 80: 15.

2.3 Characterization

Transmission electron microscopy (TEM) images were taken with a JEOL 1010 transmission electron microscope operated at 100 KV. Before TEM test, samples were dispersed in ethanol and transferred to a copper grid. Both the scanning electron microscopy (SEM) images and Energy Dispersive X-ray (EDX) analysis were taken with a JEOL 7001F scanning electron microscope equipped with an EDX detector operated at 10 kV. For SEM test, the samples were placed on conductive carbon film on SEM mount and coated with carbon using sputter coater (Quorun Tech. Co.).

2.4 BMSCs isolation and *in vitro* culture

All animal experiments were approved by the Ethics Committee at the School of Dentistry in Wuhan University, People's Republic of China. Wistar female rats were subjected to bilateral sham or OVX operation at 8-week-old, and BMSCs from either sham or OVX rats were isolated after 2 months induction. After euthanasia by sodium pentobarbital and cervical dislocation, bone marrow was flushed out of the femur and tibia by using α-MEM containing 15% fetal bovine serum (FBS) and 1% penicillin/streptomycin (P/S). Cells were cultured in a 5% CO_2 incubator at 37 ℃, the culture medium was changed every three days until the cells were passaged. BMSCs at passage 2 were used in our study.

2.5 Preparation of MBG dissolution extracts

1 mg MBG was autoclaved before use. To prepare dissolution media, the particles were soaked in 50 ml α-MEM without serum at 37 ℃ for 48 h. After filtration by 10 ml syringe with a 0.22 μm syringe filter (Millipore, US), the supernatant was collected and added with 15% FBS and 1% P/S to make the highest concentration (200μg/ml). Then 100μg/ml, 50μg/ml, and 25μg/ml concentration media were obtained by double dilution method for cell culture experiments.

2.6 Cell Counting Kit-8 (CCK-8) assay

Cell proliferation was measured by CCK-8 method according to the manufacturer's protocol. In brief, either sham or OVX BMSCs were seeded into 96-well plates at a density of 3×10^3 per well. After 24 h, the culture medium was replaced by 100 μl per well material dissolution culture medium at the concentrations of 200, 100, 50, 25, 0μg/ml for 1, 3, 5, 7 and 9 days. The CCK-8 assay was performed at each time point by replacing the culture medium with 10% CCK-8 solution at 37 °C with 5% CO_2. 1 h later, 100 μl of incubated cell suspension was transferred to a 96-well plate for optical density (OD) measurement at 490 nm by a microplate reader [29].

2.7 Fluorescence microscopy analysis

Cell culture glass slides (24-well format) were soaked in hydrochloric acid for 24h and washed by distilled water before autoclave sterilization. Then, the slides were put into the 24-well plates, and 1×10^4 sham or OVX BMSCs per well were seeded. After 24 h incubation, cell culture medium was replaced by the prepared MBG dissolution. At day 7, the slides were washed with PBS twice and fixed with 4% paraformaldehyde for 15 min at room temperature (RT), followed by another three times wash in PBS. Cells were stained with FITC-phalloidin (5μg/ml) for 1h at RT. After washing twice with PBS, samples were incubated with DAPI (10μg/ml) for 5 min at RT. The cell morphology and cytoskeletal structure were observed by fluorescent microscopy (Leica DM4000, German).

2.8 Alkaline phosphatase staining

Both sham and OVX BMSCs were seeded in 24-well plate at a density of 1×10^5 cells per well. After 24 h incubation, culture medium was replaced by MBG dissolution plus osteogenic medium containing α-MEM supplemented with 15% FBS, 10 mM sodium β-glycerol phosphate, 50μg/ml L-ascorbic acids and 1.0×10^{-8} M dexamethasone. At day 7 and 14, alkaline phosphatase (ALP) staining was performed to examine osteogenic differentiation by using the ALP staining kit, according to the manufacturer's instructions. The samples were observed under light microscopy (Leica DM IRB).

2.9 Quantitative alkaline phosphatase activity

The cell seeding density and culture procedures were the same as in ALP staining. Quantitative ALP activity was measured at day 7 and 14. At each time point, the culture media was removed and washed with PBS three times before treated with 150 μl per well of 0.3% Triton X-100. The cell suspensions were transferred to 1.5 ml tubes and centrifuged at 14000 rcf at 4 °C for 10 min. Then, 50 μl of cell lysates per well were transferred to new 96-well plates to determine the ALP activity and total amount of protein by *p*-nitrophenyl phosphate method. After 2 h incubation at 37 °C, the reaction was stopped by adding 50 μl of 1 N NaOH per sample. The reaction product was determined at 405 nm in a microplate reader. Using *p*-nitrophenol as a standard, the ALP activity was calculated based on standards curves and then normalized to the total protein content determined by BCA protein assay kit.

2.10 Alizarin red staining

The cell seeding density and culture procedures were the same as in ALP staining. 0.685 g Alizarin powder was dissolved into 50 ml distilled water, and the staining (pH=4.2) was adjusted by adding ammonium hydroxide. At day 14, cells were fixed and stained in Alizarin Red solution for 15 min and washed in distilled water to remove excess stain. The calcium nodule staining was photographed by Canon DSLR camera (Nikon Eclipse TS100) [30,31].

2.11 Oil red-O staining

Both sham or OVX BMSCs were seeded at 1.0×10^5 cells per well into 24-well plate, and the culture medium was replaced by MBG dissolution plus adipogenic medium containing α-MEM supplemented with 15% FBS, 1 mM 3-isobutyl-1-methylxanthine,10ng/ml insulin and 60μM indomethacin and 1.0×10^{-7} M dexamethasone after 24 h incubation. The medium was changed every 3 days. At day 14, the cells were fixed and stained with Oil Red solution for 10 minutes at RT. After removing excess stain, the red stained lipid droplets were photographed by light mi croscopy (Nikon Eclipse TS100).

2.12 Quantitative real-time RT-PCR

The cell seeding density and culture procedures were the same as in ALP staining. Sham and OVX BMSCs were washed with PBS and total cellular RNA was extracted using RNA kit (Omega, USA).Total RNA was reverse transcribed in accordance with the manufacturer's instructions (Takara, Japan). PCR amplification was performed in a real-time PCR system with specific primers for Runx2, PPARγ, and GAPDH. The reaction conditions for PCR were 40 cycles of denaturation at 95°C for 15s, annealing at 55°C for 34s, and extension at 72°C for 1 min. Primer sequences for differentiation markers are detailed in Table 1.

2.13 Western blotting

1×10^6 sham or OVX BMSCs were seeded per 10 cm cell culture dish. After 24h incubation, the culture medium was replaced by MBG dissolution and changed every three days till day 7 or 14. To obtain total protein, cells were lysed in ice cold RIPA lysis buffer and centrifuged at 12000 rcf for 10 min at 4°C to remove debris. Protein concentrations were determined by using BCA protein assay kit, and the protein extracts were heat denatured in SDS-PAGE sample loading buffer. Then, the protein samples were separated by 10% sodium dodecysulfate-polyacrylamide gel electrophoresis (SDS-PAGE) and transferred onto polyvinylidene fluoride (PVDF)

membranes. The membranes were then probed with primary antibodies, including anti- PPARγ (1:1000), anti-Runx2 (1:1000) and anti-β-actin (1:500) at 4°C overnight.

2.14 Statistical analysis

All samples were measured in triplicate. The results were presented as mean ± standard deviation (SD). The data were submitted to analysis of variance, and means were compared by the Student's test. Statistical significance was set to $p<0.05$.

3 Results

3.1 Characterization of MBG

The TEM image of MBG showed a highly ordered one dimensional pore channel structure with the pore size of approximately 5 nm (Fig. 1A). The SEM image illustrated the irregular particle shapes of MBG with smooth surfaces (Fig. 1B). Corresponding EDX analysis confirmed the existence of Si, Ca, and P (Inset in the Fig. 1B). The mass ratio of Si to Ca was tested to be 88: 12 according to EDX results, close to the feeding molar ratio.

3.2 Cell proliferation and morphology

The biocompatibility of sham and OVX BMSCs cultured in MBG dissolutions was evaluated by CCK-8 assay (Fig.2). Sham and OVX BMSCs showed similar proliferation pattern within 9 days of culture (Fig.2A); this finding indicated that BMSCs proliferation was not affected by the concentration of MBG dissolution. Compared with sham BMSCs, OVX BMSCs exhibited a lower viability on days 7 and 9 (Fig 2B) ($P<0.05$).

Additionally, sham and OVX BMSCs were similar in cell size. The cytoskeletons of the two BMSCs were stained on day 7 by FITC-phalloidin which presents high-affinity to actin filaments. The sham BMSCs expanded with an elongated shape,

whereas the OVX BMSCs in MBG dissolution tended to be distributed in polygonal, short, and flat shapes (Fig 3). In addition, sham BMSCs exhibited increased production of pseudopodia around the cells compared with OVX BMSCs at lower concentrations of MBG dissolution (Fig.3B and 3G).

3.3 Osteogenic and adipogenic differentiation of sham and OVX BMSCs

3.3.1 Osteogenic differentiation

Sham and OVX BMSCs were stained brown in the cytoplasmic region for ALP staining, which was highlighted by the red arrows (Fig. 4). The amount of positively stained BMSCs increased on day 14 in both groups. .

ALP activity was quantified after 7 and 14 days of induction in MBG dissolution plus osteogenic medium (Fig. 5). Sham BMSCs exhibited relatively higher levels of ALP activity than OVX BMSCs at both time points. Interestingly, the ALP levels in the various concentrations of MBG dissolution increased in a dose-dependent manner. The ALP levels reached to peak values at 50μg/ml of MBG dissolution, then significantly decreased in the highest doses of MBG dissolution (200μg/ml), except for the sham BMSCs cultured in 100μg/ml, which showed the highest ALP activity on day 14.

To further analyze cell mineralization, Alizarin Red staining was performed after 14 days of induction in MBG dissolution plus osteogenic medium (Fig. 6). Mineralized nodules were formed in all the groups, but the amount of mineralization was higher in sham BMSCs groups than in the OVX BMSCs. Additionally, moderate doses (50 and 100μg/ml) of MBG dissolution induced more mineralized matrix, showing a similar trend to the level of ALP activity.

Runx2 is a key transcription factor that regulates bone development and maintenance of the extracellular matrix [32,33]. Quantitative real-time RT-PCR results for *Runx2* mRNA expression, relative to 0 groups as a control, are shown in Fig.7. *Runx2* mRNA

expression of sham and OVX BMSCs in the various concentrations of MBG dissolution increased in a dose-dependent manner after 7 and 14 days of induction. 100μg/ml of MBG dissolution induced more *Runx2* mRNA expression in sham BMSCs (Fig. 7A and 7B). For OVX BMSCs, it reached to peak values at 25μg/ml of MBG dissolution, and significantly decreased in the highest doses of MBG dissolution (200μg/ml) on day 7 (Fig. 7A), whereas the OVX BMSCS cultured in 100μg/ml showed the highest *Runx2* mRNA expression on day 14(Fig. 7B).

The results of Western blot analysis for Runx2 protein expression was shown in Fig.8. OVX BMSCs expressed significant lower levels of Runx2 compared with sham BMSCs after treating with MBG dissolution (Fig. 8A). Densitometric analyses showed that the expression of Runx2 was statistically higher in 50 and 25μg/ml MBG dissolution than in the other groups of sham BMSCs (Fig. 8B). The MBG dissolution did not rescue the damage of osteoporosis to cells in OVX BMSCs but presented suppressive effect in accordance with the expression of Runx2 (Fig. 8B).

3.3.2 **Adipogenic differentiation**

Oil Red-O staining and Western blot were performed to investigate the effects of MBG dissolution on sham and OVX BMSCs during adipogenic differentiation. The two BMSCs showed the accumulation of positively stained lipid vacuoles in their cytoplasm in response to adipogenic induction. Sham BMSCs formed significantly higher amount of lipid vacuoles than OVX BMSCs at each concentration of MBG dissolution (Fig. 9A-9J). Interestingly, 200 and 100μg/ml MBG dissolution induced lower Oil Red-O stained area (%) in sham BMSCs group, whereas 50 and 25 μg/ml MBG dissolution showed the most significant suppression in OVX BMSCs (Fig. 9K). These results suggested that OVX BMSCs were less vulnerable to adipogenic differentiation, and a lower dose of MBG was required to dampen adipogenesis in osteoporotic condition.

PPARγ is a nuclear regulator in adipocyte growth, differentiation and metabolism [34].

Quantitative real-time RT-PCR results for *PPARγ* mRNA expression were shown in Fig.7. Interestingly, moderate doses (25 and 50μg/ml) of MBG dissolution led to a distinct decrease *PPARγ* mRNA expression as compared to that control group in both sham and OVX BMSCs. High concentration (200μg/ml) presented relatively weak decrease *PPARγ* mRNA expression of sham and OVX BMSCs (Fig.7C and 7D).

We detected the protein levels of PPARγ both in sham and OVX BMSCs cultured in MBG dissolution. Lower expression of PPARγ was found in OVX BMSCs than that in sham BMSCs (Fig.8A). Statistical suppression of PPARγ expression was observed in sham BMSCs than in the other groups in 200μg/ml concentration MBG dissolution compared to other groups (Fig.8C). Treatment with 25, 50, and 200μg/ml MBG dissolution led to a distinct decrease PPARγ expression as compared to that at 0μg/ml group in OVX BMSCs (Fig. 8C).

4 Discussion

MBG, as the third generation of biomaterials, can stimulate specific cellular responses at the molecular level [35]. MBG is considered as a promising bone substitute for bone defect healing because it release soluble Si, Ca, P and Na ions at contact surface [7]. The present study was to evaluate the dosing effects of MBG dissolution on sham and OVX BMSCs during osteogenesis and adipogenesis. Cell viability was not affected by MBG dissolution or OVX condition. In addition, both the osteogenesis and adipogenesis of BMSCs were significantly reduced under osteoporotic condition during MBG stimulation. However, moderate doses (50 and/or 100μg/ml) of MBG dissolution can better promote ALP activity and mineralization in osteoporotic and healthy models, whereas the doses (200 and/or 100μg/ml) suppressed adipogenesis of BMSCs in the healthy model.

Studies reported that Ca ion concentrations above 10mmol are cytotoxic to osteoblasts, but suitable Ca ion concentrations (2-8mmol) can promote cell proliferation [36]. For instance, P ions (10 mmol) stimulated the expression of the matrix Gla protein in

osteoblasts which is a key regulator during bone formation [37]. In the current study, we first detected the cell viability to evaluate the safe dosing range (0-200μg/ml) of MBG dissolution. No statistical difference was found in cell proliferation after culturing in the tested ranges of MBG dissolution. In addition, OVX BMSCs proliferated slower than sham BMSCs on days 7 and 9, indicating a defective potential of regeneration in osteoporosis. Moreover, BMSCs differentiation was accompanied by considerable alterations in morphological and cytoskeletal rearrangements. BMSCs changed from a characteristic typical spindle shape towards a spherical form[2] . By contrast, sham and OVX BMSCs cultured without MBG dissolution maintained a slender shape. The morphological changes might have resulted from the effect of the released Si, Ca, P, and Na ions.

ALP, a specific extracellular enzyme secreted by active osteoblasts, can directly participate in the synthesis and mineralization of bone matrix [38]. The present results showed that the osteogenic potential of OVX BMSCs was lower than that of sham BMSCs, and the moderate doses (50-100μg/ml) of MBG dissolution presented an optimal effect on ALP activity and matrix mineralization. We hypothesized that those differences are probably attributed to the ions released by MBG. Bioglass releases ions involved in the bone metabolism and plays a physiological role in angiogenesis, bone tissue growth and mineralization [39,40]. For instance, Ca ions can directly activate intracellular Ca-sensing receptors in osteoblasts [41]; Si ions can promote mineralization [42] and osseointegration [43] at the initiation stage of bone formation, which is probably ascribed to the effects on collagen I and osteopontin synthesis [44]. P ions can upregulate Glvr-1 and Glvr-2 in odontoblast-like cells and ERK1/2 phosphorylation, as well as promote CaP crystalization [45]. Moreover, the released ions can result in an increased pH environment which favors the precipitation of the CaP surface layer [46]. Finally, MBG dissolutions can accelerate the osteoblasts cell cycle through the transition from G0 to G1 stages, and the MBG substrate could also accelerate cell proliferation in S phase and G2-M phase [47].

Runx2 regulates osteoblastic and chondrogenic cell differentiation [25]during bone formation. Komori et al. first reported that Runx $2^{-/-}$ displayed a complete lack of intramembranous and endochondral ossification because of the immature osteoblasts [48]. In our study, the mRNA expression of *Runx2* of sham BMSCs was relatively upregulated after moderate concentration (50-100μg/ml) of MBG dissolution stimulation compared to 0μg/ml control group. Moreover, the protein expression of Runx2 was expressed 5-10 times higher in sham BMSCs than in OVX BMSCs. Afterward, 25 and 50μg/ml of MBG dissolution statistically enhanced Runx2 expression in sham BMSCs. However, all concentrations of the MBG dissolution slightly decreased the protein expression of Runx2 in OVX BMSCs after 14 days osteogenic induction. Other transcription factors such as transcriptional activator PDZ-binding motif(TAZ)[49] and osterix [50] also demonstrated a proosteogenic and antiadipogenic relationship. We hypothesized that the other transcription factors were activated by the MBG dissolution induction in the osteoporotic model.

Osteoblasts and adipocytes originated from a common precursor MSCs, and an inverse correlation existed between adipogenesis and osteogenesis [51]. BMSC adipogenesis undergoes the determination phase and terminal differentiation phase [52]. Preadipocytes show fibroblastic morphology in determination phase, but differentiate into adipocytes and acquire lipid synthesis and storage function during the terminal phase of differentiation. The positively stained lipid vacuoles in the cytoplasm of sham and OVX BMSCs showed the adipogenic terminal differentiation phase after 14 days of induction [53]. The main cause of pathogenesis in primary osteoporosis is the senescence of BMSCs, leading to decrease in proliferation and differentiation[54]. The senescence of BMSCs gradually affects BMSCs stem-like properties and finally damages potential to engage in multiple differentiation[54,55]. Thus, OVX BMSCs exhibited lower adipogenic potential than sham BMSCs, possibly because of their damaged differentiation capacity. 50μg/ml MBG dissolution can significantly suppress OVX BMSCs adipogenesis, while 200μg/ml and 100μg/ml MBG dissolution reduced the adipogenesis in sham BMSCs.

PPARγ is the master regulator of adipogenesis and has been well described for its anti-osteoblastogenic effects [24]. All concentration of MBG dissolution showed relatively inhibition effect on the mRNA expression of *PPARγ* in sham and OVX BMSCs at day 7 and 14 compared to 0μg/ml control group, especially the moderate concentration (25-50μg/ml) of MBG dissolution. Sham BMSCs showed an enhanced level of PPARγ expression compared with OVX BMSCs, which further confirmed the defective adipogenic phenotype in osteoporotic condition according to the Oil Red-O staining results. The MBG dissolution demonstrated a strong anti-adipogenic effect on OVX BMSCs, but only 200μg/ml MBG dissolution showed statistical difference in sham BMSCs. These phemonena can be explained by an increased production of bone marrow adipocytes counterbalanced with a dimished amount of osteogenic cells in osteoporotic patients[56]. The imbalance between adipogenesis and osteogenesis has been shown to be associated with obesity and osteoporosis [57,58]. Previous studies reported that osteopontin can regulate BMSCs differentiation by inhibiting C/EBPs signaling which plays an important role in directing adipogenesis and osteogenesis [59]. In this study, the MBG released ions that contributed to the regulation of osteogenesis and adipogenesis in both healthy and osteoporotic conditions.

Conclusion

The osteogenic and adipogenic potentials of BMSCs were significantly declined in osteoporotic condition. MBG dissolution at 50-100μg/ml of MBG dissolution can promote osteogenesis in BMSCs of healthy and osteoporotic models, while 200-100μg/ml of MBG dissolution suppressing adipogenesis of BMSCs in healthy models and 25-50μg/ml MBG dissolution suppressing adipogenesis of BMSCs in osteoporotic models. These results suggest the potential of MBG as potential candidate for bone substitutes in the future applications.

Acknowledgements

This research was financially supported by the National Natural Science Foundation of China (81170992)

Notes

[#] Authors contributed equally to this work.

References

1. Hench LL. The story of Bioglass ®. Journal of Materials Science Materials in Medicine 2006;17(11):967-978.
2. Rodríguez JP, González M, Ríos S, Cambiazo V. Cytoskeletal organization of human mesenchymal stem cells (MSC) changes during their osteogenic differentiation. Journal of Cellular Biochemistry 2004;93(4):721–731.
3. Wu T, Tan L, Cheng N, Yan Q, Zhang YF, Liu CJ, Shi B. PNIPAAM modified mesoporous hydroxyapatite for sustained osteogenic drug release and promoting cell attachment. Mater Sci Eng C Mater Biol Appl 2016;62:888-96.
4. Wei X, Jiang C. Well-ordered mesoporous bioactive glasses (MBG): a promising bioactive drug delivery system. Journal of Controlled Release Official Journal of the Controlled Release Society 2006;110(3):522-30.
5. Newby PJ, El-Gendy R, ., Kirkham J, ., Yang XB, Thompson ID, Boccaccini AR. Ag-doped 45S5 Bioglass?-based bone scaffolds by molten salt ion exchange: processing and characterisation. Journal of Materials Science Materials in Medicine 2011;22(3):557-569.
6. Caridade SG, Merino EG, Alves NM, Mano JOF. Bioactivity and viscoelastic characterization of chitosan/bioglass? composite membranes. Macromolecular Bioscience 2012;12(8):1106-13.
7. Hench LL, Polak JM. Third-generation biomedical materials. Science 2002;295(5557):1014-1017.
8. Cheng N, Wang Y, Zhang Y, Shi B. The osteogenic potential of mesoporous bioglasses/silk and non-mesoporous bioglasses/silk scaffolds in ovariectomized rats: in vitro and in vivo evaluation. PLoS One 2013;8(11):e81014.
9. Zhang Y, Cheng N, Miron R, Shi B, Cheng X. Delivery of PDGF-B and BMP-7 by mesoporous bioglass/silk fibrin scaffolds for the repair of osteoporotic defects. Biomaterials 2012;33(28):6698-708.
10. Reilly GC, Shula R, Chen AT, Paul D. Differential alkaline phosphatase responses of rat and human bone marrow derived mesenchymal stem cells to 45S5 bioactive glass. Biomaterials 2007;28(28):4091-7.
11. Tsigkou O, Jones JR, Polak JM, Stevens MM. Differentiation of fetal osteoblasts and formation of mineralized bone nodules by 45S5 Bioglass conditioned medium in the absence of osteogenic supplements. Biomaterials 2009;30(21):3542-50.
12. NIH Consensus Development Panel on Osteoporosis Prevention, Diagnosis, and Therapy, March 7-29, 2000: highlights of the conference. South Med J 2001;94(6):569-73.
13. Arumugan S, Bikramjit B, Shenoy SJ, Zahira J, Naresh S, Artemis S. Early osseointegration of a strontium containing glass ceramic in a rabbit model. Biomaterials 2013;34(37):9278-9286.
14. Kalu DN. The ovariectomized rat model of postmenopausal bone loss. Bone & Mineral 1992;15(3):175-91.
15. Cheng N, Dai J, Cheng X, Li S, Miron RJ, Wu T, Chen W, Zhang Y, Shi B. Porous CaP/silk composite scaffolds to repair femur defects in an osteoporotic model. J Mater Sci Mater Med 2013;24(8):1963-75.
16. Martin RB, Zissimos SL. Relationships between marrow fat and bone turnover in ovariectomized and intact rats. Bone 1991;12(2):123-31.
17. Kawai K, ., Tamaki A, ., Hirohata K, . Steroid-induced accumulation of lipid in the osteocytes of

the rabbit femoral head. A histochemical and electron microscopic study. Journal of Bone & Joint Surgery American Volume 1985;67(5):755-63.

18. Zou D, Zhang Z, He J, Zhu S, Wang S, Zhang W, Zhou J, Xu Y, Huang Y, Wang Y and others. Repairing critical-sized calvarial defects with BMSCs modified by a constitutively active form of hypoxia-inducible factor-1alpha and a phosphate cement scaffold. Biomaterials 2011;32(36):9707-18.
19. Lim SK, Cho H, Lee EK, Won Y, Kim C, Ahn W, Lee EA, Son Y. Osteogenic stimulation of human adipose-derived stem cells by pre-treatment with fibroblast growth factor 2. Cell & Tissue Research 2015;104(707):1-11.
20. Connelly JT, Petrie TA, Garcia AJ, Levenston ME. Fibronectin- and collagen-mimetic ligands regulate bone marrow stromal cell chondrogenesis in three-dimensional hydrogels. Eur Cell Mater 2011;22:168-76; discussion 176-7.
21. Liu H, Peng H, Wu Y, Zhang C, Cai Y, Xu G, Li Q, Chen X, Ji J, Zhang Y and others. The promotion of bone regeneration by nanofibrous hydroxyapatite/chitosan scaffolds by effects on integrin-BMP/Smad signaling pathway in BMSCs. Biomaterials 2013;34(18):4404-17.
22. Griffin M, ., Iqbal SA, Bayat A, . Exploring the application of mesenchymal stem cells in bone repair and regeneration. Journal of Bone & Joint Surgery British Volume 2011;93(4):427-434.
23. Dragojevič J, Logar DB, Komadina R, Marc J. Osteoblastogenesis and Adipogenesis Are Higher in Osteoarthritic than in Osteoporotic Bone Tissue. Archives of Medical Research 2011;42(5):392-7.
24. James AW. Review of Signaling Pathways Governing MSC Osteogenic and Adipogenic Differentiation. Scientifica 2013;2013(1):684736-684736.
25. Yoshida CA, Yamamoto HT, Furuichi T, Ito K, Inoue K, Yamana K, Zanma A, Takada K, Ito Y, Komori T. Runx2 and Runx3 are essential for chondrocyte maturation, and Runx2 regulates limb growth through induction of Indian hedgehog. Genes & Development 2004;18(8):págs. 952-963.
26. Ph.D. CGMD, Cawthorn WP, Yan L, Zhao G, Macdougald OA, Franceschi RT. Reciprocal Control of Osteogenic and Adipogenic Differentiation by ERK/MAP Kinase Phosphorylation of Runx2 and PPARγ Transcription Factors †. Journal of Cellular Physiology 2016;231(3).
27. Xiaoxia Y, Chengzhong Y, Xufeng Z, Jiawei T, Dongyuan Z. Highly ordered mesoporous bioactive glasses with superior in vitro bone-forming bioactivities. Angewandte Chemie International Edition 2004;43(43):5980-4.
28. Yan X, Yu C, Zhou X, Tang J, Zhao D. Highly ordered mesoporous bioactive glasses with superior in vitro bone-forming bioactivities. Angew Chem Int Ed Engl 2004;43(44):5980-4.
29. Zhang Z, Han Y, Song J, Luo R, Jin X, Mu D, Su S, Ji X, Ren YF, Liu H. Interferon-gamma regulates the function of mesenchymal stem cells from oral lichen planus via indoleamine 2,3-dioxygenase activity. J Oral Pathol Med 2015;44(1):15-27.
30. Alkhalil M, Smajilagic A, Redzic A. Human dental pulp mesenchymal stem cells isolation and osteoblast differentiation. Med Glas (Zenica) 2015;12(1):27-32.
31. Castren E, Sillat T, Oja S, Noro A, Laitinen A, Konttinen YT, Lehenkari P, Hukkanen M, Korhonen M. Osteogenic differentiation of mesenchymal stromal cells in two-dimensional and three-dimensional cultures without animal serum. Stem Cell Res Ther 2015;6:167.
32. Kundu M, Javed A, Jeon JP, Horner A, Shum L, Eckhaus M, Muenke M, Lian JB, Yang Y, Nuckolls GH and others. Cbfbeta interacts with Runx2 and has a critical role in bone development. Nat

Genet 2002;32(4):639-44.

33. Jonason JH, Xiao G, Zhang M, Xing L, Chen D. Post-translational Regulation of Runx2 in Bone and Cartilage. J Dent Res 2009;88(8):693-703.
34. Rosen ED, Spiegelman BM. PPARgamma : a nuclear regulator of metabolism, differentiation, and cell growth. J Biol Chem 2001;276(41):37731-4.
35. Narayan RJ. The next generation of biomaterial development. Philosophical Transactions 2010;368(1917):1831.
36. Maeno S, Niki Y, Matsumoto H, Morioka H, Yatabe T, Funayama A, Toyama Y, Taguchi T, Tanaka J. The effect of calcium ion concentration on osteoblast viability, proliferation and differentiation in monolayer and 3D culture. Biomaterials 2005;26(23):4847-55.
37. Khoshniat S, Bourgine A, Julien M, Petit M, Pilet P, Rouillon T, Masson M, Gatius M, Weiss P, Guicheux J. Phosphate-dependent stimulation of MGP and OPN expression in osteoblasts via the ERK1/2 pathway is modulated by calcium. Journal of Biological Chemistry 2012;287(43):36168-36178.
38. Franceschi RT, Chunxi GE, Xiao G, Hernan R, Jiang DI. Transcriptional Regulation of Osteoblasts. Annals of the New York Academy of Sciences 2007;1116(1-4):196-207.
39. Xynos ID, Edgar AJ, Buttery LD, Hench LL, Polak JM. Ionic products of bioactive glass dissolution increase proliferation of human osteoblasts and induce insulin-like growth factor II mRNA expression and protein synthesis. Biochemical & Biophysical Research Communications 2000;276(2):461-465.
40. Hoppe A, Güldal NS, Boccaccini AR. A review of the biological response to ionic dissolution products from bioactive glasses and glass-ceramics. Biomaterials 2011;32(11):2757-74.
41. Marie PJ. The calcium-sensing receptor in bone cells: A potential therapeutic target in osteoporosis. Bone 2009;46(3):571-6.
42. Carlisle EM. Silicon: a possible factor in bone calcification. Science 1970;167(3916):279-80.
43. Xu S, Lin K, Wang Z, Chang J, Wang L, Lu J, Ning C. Reconstruction of calvarial defect of rabbits using porous calcium silicate bioactive ceramics. Biomaterials 2008;29(17):2588-96.
44. D M R, N O, R J, H F J C, B A J E, R P H T, J J P, G N H. Orthosilicic acid stimulates collagen type 1 synthesis and osteoblastic differentiation in human osteoblast-like cells in vitro. Bone 2003;32(2):127–135.
45. Wittrant Y, ., Bourgine A, ., Khoshniat S, ., Alliot-Licht B, ., Masson M, ., Gatius M, ., Rouillon T, ., Weiss P, ., Beck L, ., Guicheux J, . Inorganic phosphate regulates Glvr-1 and -2 expression: role of calcium and ERK1/2. Biochemical & Biophysical Research Communications 2009;381(2):259–263.
46. Cerruti M, Greenspan D, Powers K. Effect of pH and ionic strength on the reactivity of Bioglass ® 45S5. Biomaterials 2005;26(14):1665-1674.
47. Hench LL, Polak JM, Xynos ID, Buttery LDK. Bioactive materials to control cell cycle. Material Research Innovations 2000;3(6):313-323.
48. Komori T, ., Yagi H, ., Nomura S, ., Yamaguchi A, ., Sasaki K, ., Deguchi K, ., Shimizu Y, ., Bronson RT, Gao YH, Inada M, . Targeted disruption of Cbfa1 results in a complete lack of bone formation owing to maturational arrest of osteoblasts. Cell 1997;89(5):755-64.
49. Zhang Y, Wang Z, Ding L, Damaolar A, Li Z, Qiu Y, Yin Z. Lentivirus-TAZ Administration Alleviates Osteoporotic Phenotypes in the Femoral Neck of Ovariectomized Rats. Cellular Physiology & Biochemistry 2016;38(1):283-294.

50. Lee YJ, Park SY, Lee SJ, Boo YC, Choi JY, Kim JE. Ucma, a direct transcriptional target of Runx2 and Osterix, promotes osteoblast differentiation and nodule formation. Osteoarthritis & Cartilage 2015;23(8):1421-1431.
51. Liming P, Peter T. Fat's loss is bone's gain. Journal of Clinical Investigation 2004;113(6):805.
52. Muruganandan S, ., Roman AA, Sinal CJ. Adipocyte differentiation of bone marrow-derived mesenchymal stem cells: cross talk with the osteoblastogenic program. International Journal of Cardiovascular Interventions 2009;3(2):111-120.
53. Rosen ED, Macdougald OA. Adipocyte differentiation from the inside out. Nature Reviews Molecular Cell Biology 2006;7(12):885-896.
54. Li C, Wei G, Gu Q, Wang Q, Tao S, Xu L. Proliferation and differentiation of rat osteoporosis mesenchymal stem cells (MSCs) after telomerase reverse transcriptase (TERT) transfection. Medical Science Monitor International Medical Journal of Experimental & Clinical Research 2014;21:845-854.
55. Gao Y, Jiao Y, Nie W, Lian B, Wang B. In vitro proliferation and differentiation potential of bone marrow-derived mesenchymal stem cells from ovariectomized rats. J.agric.food Chem 2014;46(6):1794-1799.
56. J Pablo R, Pablo A, Susana R, Ana María P. Involvement of adipogenic potential of human bone marrow mesenchymal stem cells (MSCs) in osteoporosis. Current Stem Cell Research & Therapy 2008;3(3):208-218(11).
57. Gomez-Ambrosi J, Rodriguez A, Catalan V, Fruhbeck G. The bone-adipose axis in obesity and weight loss. Obes Surg 2008;18(9):1134-43.
58. Wronski TJ, Lowry PL, Walsh CC, Ignaszewski LA. Skeletal alterations in ovariectomized rats. Calcif Tissue Int 1985;37(3):324-8.
59. Chen Q, Shou P, Zhang L, Xu C, Zheng C, Han Y, Li W, Huang Y, Zhang X, Shao C. An Osteopontin-Integrin Interaction Plays a Critical Role in Directing Adipogenesis and Osteogenesis by Mesenchymal Stem Cells. Stem Cells 2014;32(2):327-337.

Table 1 The primers used for real-time RT-PCR (GAPDH was used as a housekeeping gene)

Primer	Sequences 5′ -3′
RUNX2	Forward: ATCCAGCCACCTTCACTTACACC
	Reverse: GGGACCATTGGGAACTGATAGG
PPARγ	Forward: CGC TGA TGC ACT GCC TAT GA
	Reverse: GGG CCA GAA TGG CAT CTC T
GAPDH	Forward: AGAAGGTGGTGAAGCAGGCGG
	Reverse: ATCCTTGCTGGGCTGGGTGG

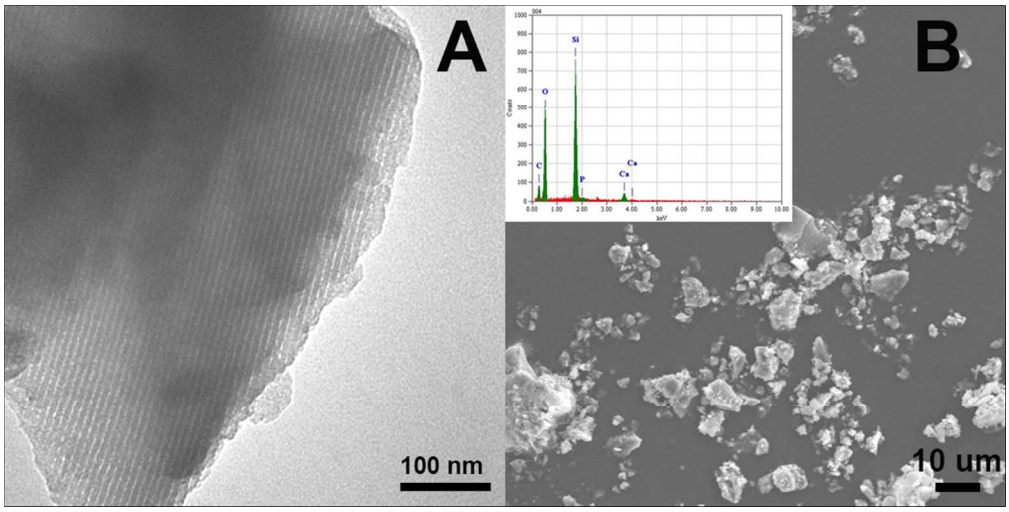

Fig. 1 TEM (A) and SEM (B) image of MBGs. Inset in B is the corresponding EDS pattern.
Fig.1
254x127mm (300 x 300 DPI)

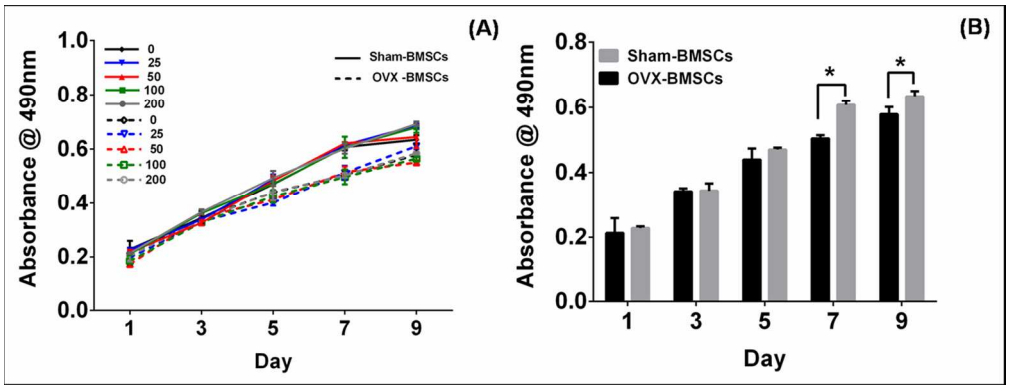

Fig. 2 CCK-8 assay: Sham and OVX BMSCs (A) cultured in different concentration of MBGs dissolution medium (0, 25, 50, 100 and 200 μg/ml) at day 1, 3, 5, and 9. Sham and OVX BMSCs cultured in α-MEM culture medium at day 1, 3, 5, 7 and 9 (B). (n=4 in each group; * P<0.05)
Fig. 2
69x26mm (600 x 600 DPI)

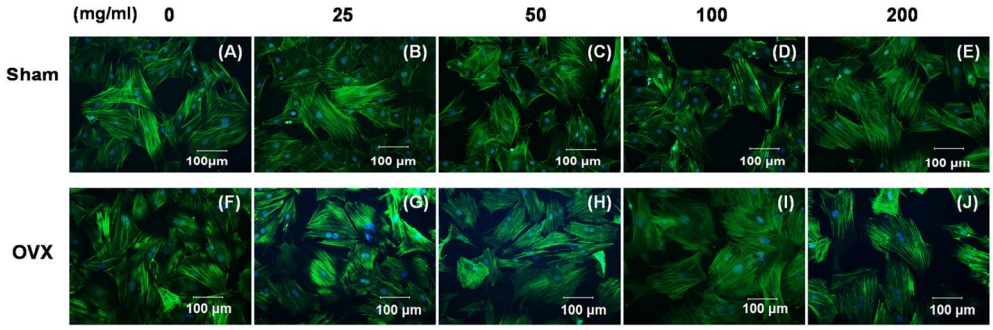

Fig. 3 Cytoskeletal morphology of sham BMSCs (A, B, C, D, E) and OVX BMSCs (F, G, H, I, J) cultured in different concentration of MBGs dissolution medium (0, 25, 50, 100 and 200 μg/ml) at day 7 under fluorescence microscopy.
Fig. 3
69x23mm (600 x 600 DPI)

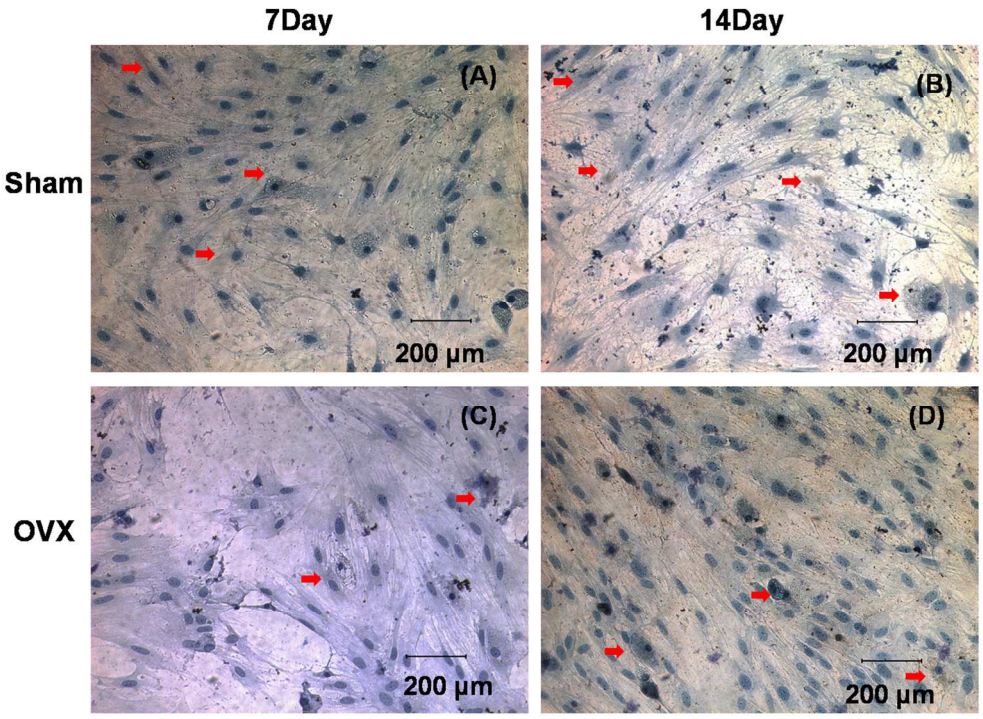

Fig. 4 Alkaline phosphatase staining of sham BMSCs (A, B) and OVX BMSCs (C, D) , which were stained brown in cytoplasmic region cultured in osteogenic induction medium at day 7 and 14.
Fig. 4
99x72mm (600 x 600 DPI)

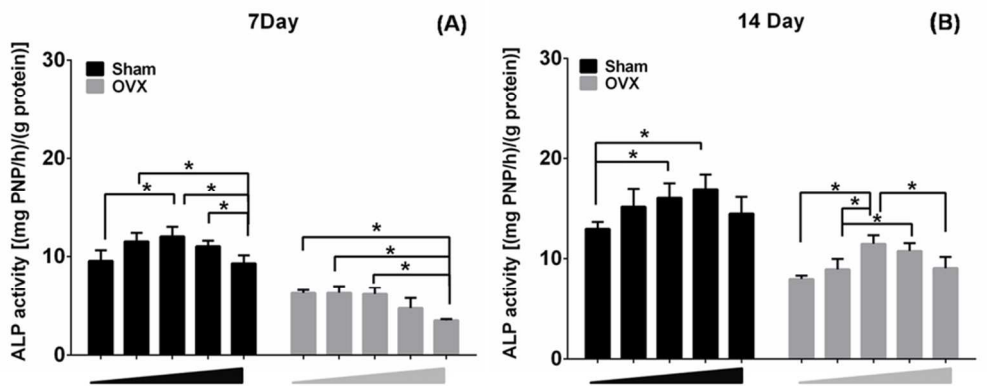

Fig. 5 Quantitative ALP activity of sham and OVX BMSCs cultured in different concentration of MBGs dissolution medium (0, 25, 50, 100 and 200 μg/ml) at day 7(A) and 14 (B). (n=3 in each group; * P<0.05)
Fig. 5
40x15mm (600 x 600 DPI)

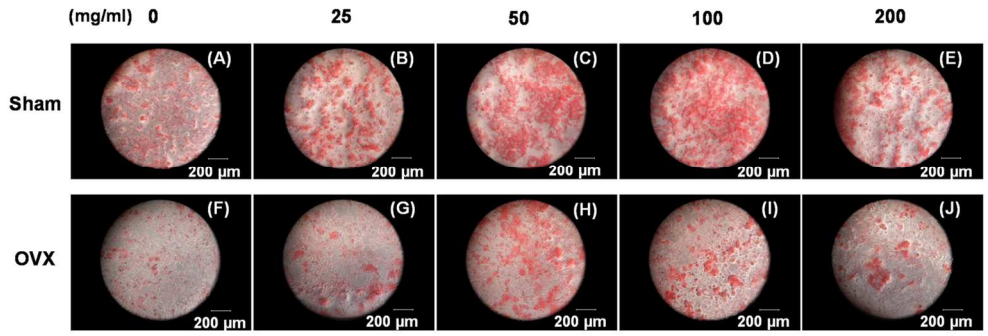

Fig. 6 Alizarin red staining of sham BMSCs (A, B, C, D, E) and OVX BMSCs (F, G, H, I, J) cultured in different concentration of MBGs dissolution medium (0, 25, 50, 100 and 200 μg/ml) under osteogenic induction for 14 days.
Fig. 6
71x23mm (600 x 600 DPI)

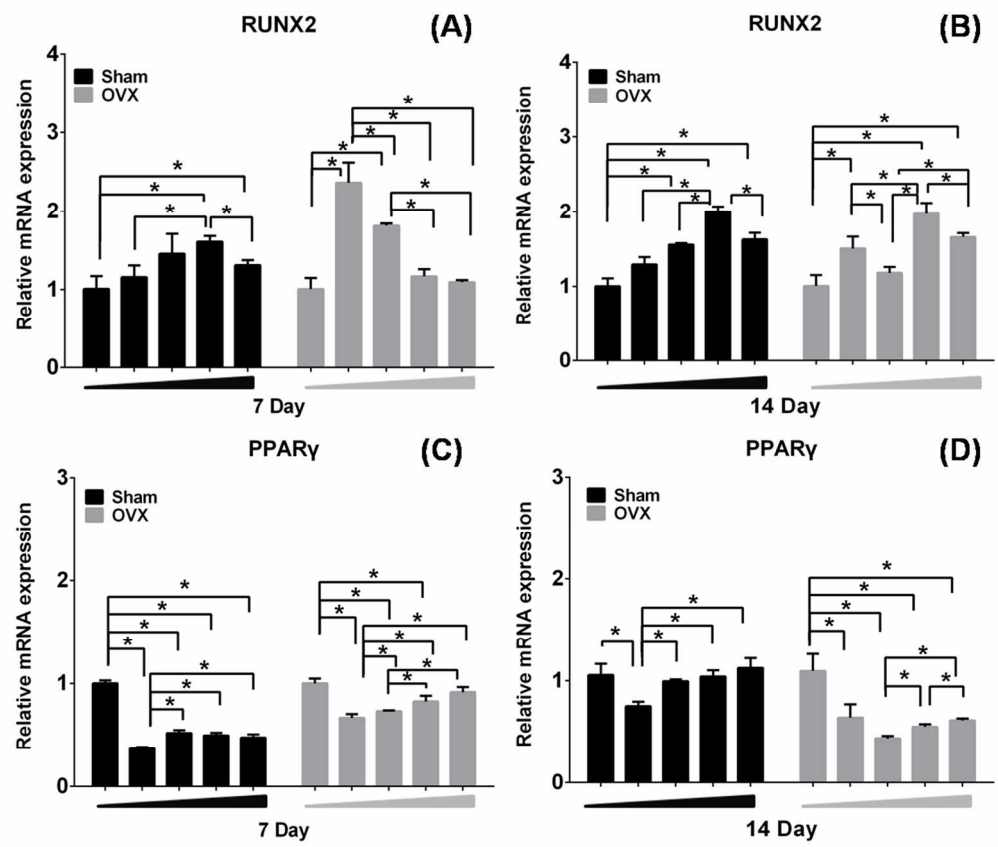

Fig.7 Real-time PCR analysis of gene Runx2 and PPARγ in sham and OVX BMSCs in different concentration of MBG extract medium (0, 25, 50, 100 and 200 μg/ml) under osteogenic induction for 7 (A, C) of 14 days (B, D). (n=3 per group; * $P<0.05$)

Fig.7

90x77mm (600 x 600 DPI)

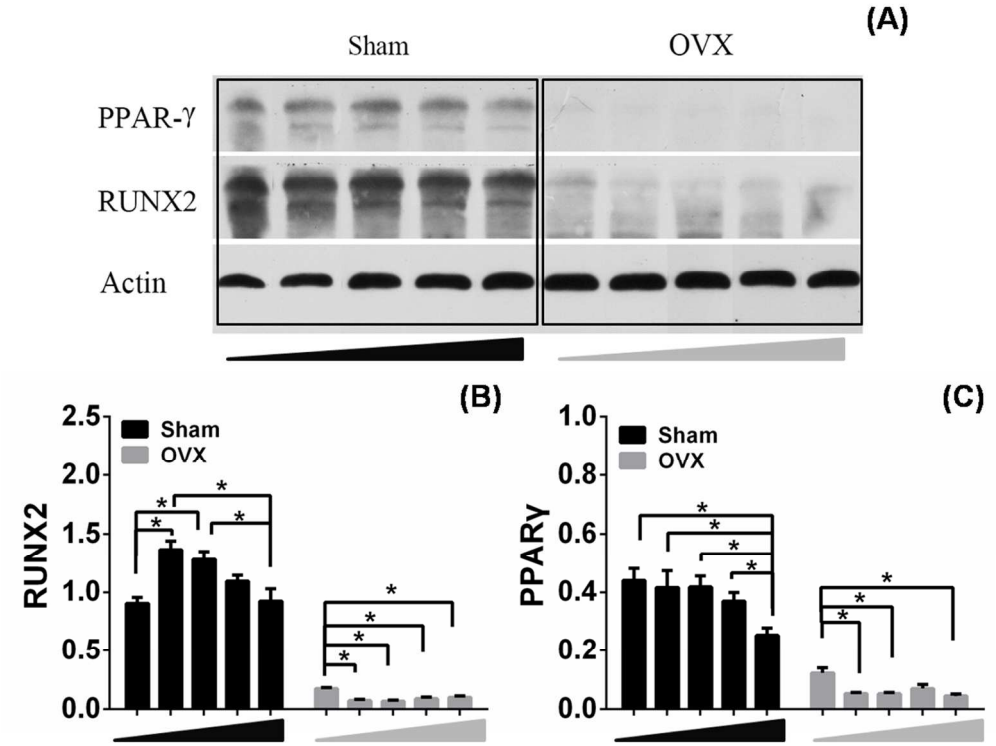

Fig. 8 The protein expression of PPARγ and Runx2 in sham and OVX BMSCs cultured in different concentration MBGs dissolution medium (0, 25, 50, 100 and 200 μg/ml) for 14 days (A). Densitometric analysis for the protein expression of Runx2(B). Densitometric analysis for the protein expression of PPARγ(C)
Fig. 8
95x72mm (600 x 600 DPI)

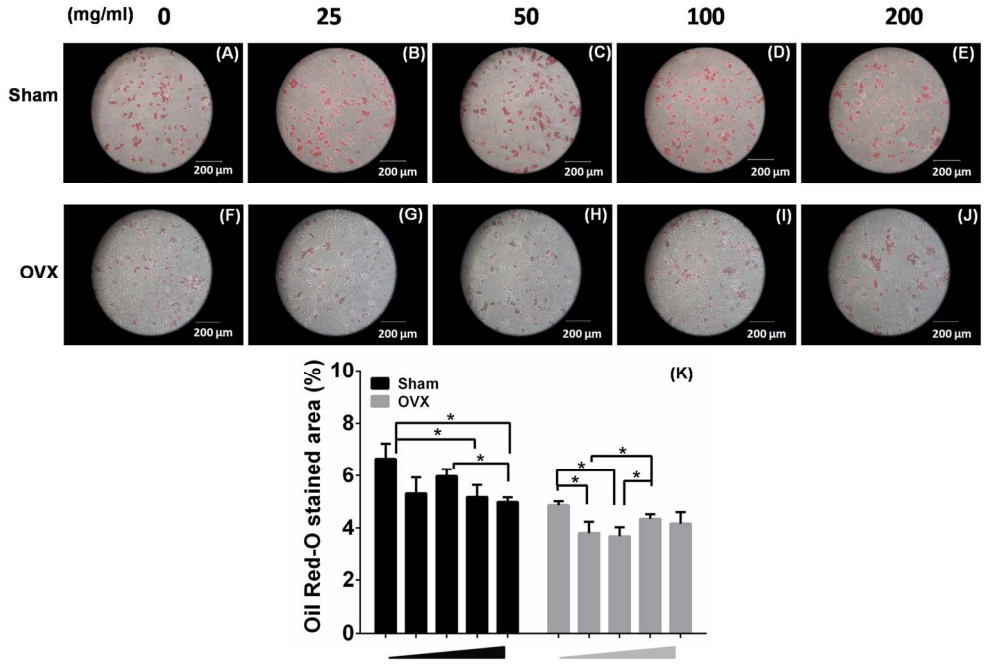

Fig. 9 Oil Red-O staining of sham BMSCs (A, B, C, D, E) and OVX BMSCs (F, G, H, I, J) cultured in different concentration of MBGs dissolution medium (0, 25, 50, 100 and 200 µg/ml) under adipogenic induction for 14 days.) (K) Percentage of (+) Oil red staining in sham or OVX BMSCs (n=3 per group; * P<0.05)
Fig. 9
84x56mm (600 x 600 DPI)